Supplement to "Seasonal dispersal of fjord meltwaters as an important source of iron and manganese to coastal Antarctic phytoplankton"

Supplemental Methods: Estimating particulate matter crustal and authigenic fractions

To estimate the fractional contribution of crustal, biogenic, and authigenic particulate matter in our samples using equation 4, we first identify the geochemical composition of the weathered source bedrock surrounding Andvord Bay. It is known that there is widespread volcanism and metamorphism (Jordan, Riley and Siddoway, 2020), and thus, ratios (Me:Al, where Me is either Fe or Mn) should reflect basaltic and andesitic crusts. However, uncertainty of the source of weathered particulate matter leads us to use average upper continental crust values (Table 1), although any contribution of a volcanic source would lead to some enrichment of TpFe and TpMn relative to TpAl and a greater estimate of the crustal contribution. Equation 4 allows for the calculation of the crustal contribution:

$$\%crustal = ([TpAl]_{sample} * Me{:}Al_{crustal})/[TpMe]_{sample} \quad (4)$$

After accounting for a biological contribution based on Me:P quotas for Fe-replete diatom cultures (0% for all samples, data not shown), we then assume the remaining particulate fraction to be authigenic.

Supplemental Methods: Limitations of surface meltwater dye experiment

When we examine the time series derived from the model, we find the model consistently underestimates the contribution of meltwater to the surface (Fig. S8). The MWf does not exceed 0.0013 at either S3 or GS stations, and its seasonal maximum of 0.0046 is found at IBB in early February. Since processes like melting of drifting icebergs and sea ice cannot be captured in the model, the applied meltwater flux is based on a simplified representation of all new freshwater sources except for precipitation in Andvord Bay. These sources include, for example, surface runoff and local melt of glacial ice exposed to the atmosphere. The flux which best recreates observed salinity and temperature profiles in Andvord Bay was achieved by a meltwater input of 0.15 GT over 4 months (Hahn-Woernle *et al.*, 2020).

The overall low modeled meltwater fraction is likely a consequence of multiple factors of which we discuss three. First, the meltwater was tracked only for the field season. The generally low salinity in the upper layer at the beginning of the season and the presence of meltwater dye at the end of the summer season (fjord average of 0.0003 MWf in upper 20m) suggested that meltwater can reside for multiple years in the fjord and cannot be fully captured by our meltwater dye. Second, local melt of glacial ice, e.g. floating icebergs, caused by a summertime surface heat flux, can have a strong impact on the MWf in the surface layer and is likely to be underestimated and not well-represented with the parameterization of the modeled

meltwater input. Third, only meltwater from the inner Andvord Bay is tracked and other sources are neglected. Based on other modeled meltwater dyes that track sources just outside Andvord Bay, the impact of the external sources is minor (maximum of 0.0003 MWf in early February) compared to the local sources, but they still contribute to the seasonal increase in MWf.

Supplemental Methods: Estimating total surface meltwater export from WAP fjords

To estimate the meltwater export resulting from a single katabatic wind event along the WAP, we first identify two fjord types: 1) fjords where waters are below the freezing temperature (cold-water); and 2) fjords where intrusions of modified UCDW reach the glacier terminus (warm-water). This distinction leads to different MWf production rates. We use data collected from Andvord Bay as a basis for export occurring in cold-water fjords. In this instance, a maximum MWf or 0.025 was observed, which corresponded to an export of 38×10^7 m^3 glacial meltwater and is based on the glacial meltwater dye export across the mouth of Andvord Bay integrated over the duration of a week-long katabatic wind event.

Meltwater runoff from glaciers due to warm atmospheric temperatures is parameterized as a function of number of days above a temperature threshold (Smith *et al.,* 1998). The area of the glacier in contact with the atmosphere predicts how much meltwater is generated. We use this simple relationship with surface area and relate it to the MWf we observe, allowing us to estimate the fractional contribution from each glacier in Andvord Bay. As an example, Bagshawe Glacier has an area of 250 km^2, which is 48% of the total glacier area for this fjord, and so would be responsible for producing 48% of the surface glacial meltwater (~18.4×10^7 m^3). By dividing the total surface glacial meltwater export for a single katabatic wind event by the total area of glaciers in Andvord Bay, we calculate the export rate of meltwater in Andvord Bay glaciers to be 7.4×10^5 m^3 km^{-2} assuming glaciers have an equal rate of meltwater production per unit area. We use this rate as representative for cold-water type glaciers.

Since warm atmospheric temperatures in contact with the glacier surface cause production of meltwater, which enters the ocean as surface runoff, this seems a reasonable assumption. Additionally, intrusions of modified UCDW can reach the glacier terminus, causing slightly higher fractions of meltwater at the surface (~0.06 in Barilari Bay). Our general model results showed exchange with water outside of the fjord occurred during katabatic wind events, including inflow of water masses at depth located from outside of the fjord. Thus, these events are likely to enhance delivery of modified UCDW to the glacier terminus (Jackson *et al*., 2014). We scale the meltwater export to the meltwater fraction since both Barilari and Andvord Bays had similar mixed layer depths. Also, ~40% export of meltwater during katabatic wind events in our model is reasonable compared to estimates for Arctic fjords (10-50%, Jackson *et al*., 2014). Based on the area of glaciers in Barilari, we calculate an export rate of meltwater for representative warm-water glaciers to be 10.2×10^5 m^3 km^{-2}. We extrapolate these rough estimates for all glaciers on the western coast of the WAP identified by Cook et al. (2016). All glaciers to the south of Andvord Bay are considered warm-water, while those to the north are cold-water (Fig. S9). The area of each of the glaciers used here is published in Cook *et al.* (2016).

Summing the entire volume export of surface glacial meltwater, we find that if all surface waters along the western coast of the WAP experienced a single katabatic wind event, reminiscent of the one recorded in Andvord Bay, a total of 3.6 x 10^{10} m^3 (36 km^3) of surface glacial meltwater is exported towards the continental shelf (5 km^3 from cold-water glaciers; 31 km^3 from warm-water glaciers). This latitudinal difference is consistent with greater meltwater fractions found on the continental shelf in the southern lines of the PAL LTER grid (Annett et al. 2017). Based on a recent compilation of TDFe content in icebergs from Antarctica (Hopwood et al. 2019), and including two measurements from our study, we use a median concentration of 544 nM (n = 57). We then assume a rough estimate for 10% of TDFe as the dissolved phase, which yields a dFe content of glacial meltwater to be 54.4 nM. This is close to our average dFe measured for three glacial ice pieces in this study (71±121 nM). To our knowledge, there are no other measurements of dMn in glacial ice, so we use our mean for three glacial ice pieces from this study (49±82 nM). We estimate a single wind event lasting one week on the western coast of the WAP corresponds to an export of 2.0 x 10^6 mol dFe and 1.8 x 10^6 mol dMn.

We realize this analysis does not take in to account the impact of shallow sills in fjords that might be important for restricting UCDW from entering the fjord mouth and interacting with glaciers. Invigorated upwelling due to buoyant plumes originating at the glacier face is expected to have a positive feedback on the melting of the glacier terminus by increasing the delivery of modified UCDW to glaciers and enhancing melt (Cape *et al.,* 2019). This may be driven by warm ocean temperatures, directly melting the face of the glaciers, or atmospheric warming could increase drainage of surface melt to the base of the glacier, resulting in subglacial discharge and buoyant plumes driving circulation. Directionality of the katabatic winds is an important parameter for wind forcing in fjords surrounded by steep topographic features (Lundesgaard *et al.,* 2018). We have explored the possibility when one katabatic wind event per year occurs in the along-fjord direction (seaward) for the entire western coast of the WAP. These mechanisms are fjord specific and deserve further attention due to the complex interactions between the ice, ocean, and atmosphere. We also concede that areal extent of glaciers may not be the most representative measure for meltwater production, when in fact glacier flow velocities might better correlate with meltwater production rates, and thus, meltwater export rates. However, the interplay between surface melt and the subglacial hydrological system, and thus flow rates could mean this is a sufficient, albeit rough assumption. Finally, large uncertainties exist for the average glacial ice content of dFe and the degree to which TDFe may be solubilized and made bioavailable. This analysis does not take into account the large quantities of solid ice (i.e., icebergs) exported via this mechanism.

Supplemental Figures and Tables

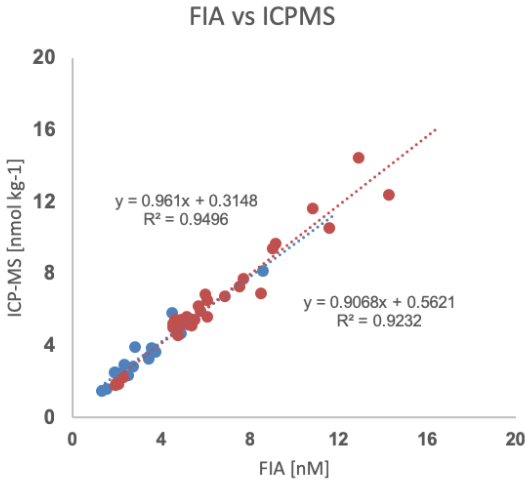

Figure S1. Comparison of analytical detection methods used for the determination of dissolved Fe (FIA versus ICP-MS). The red line denotes the 1:1.

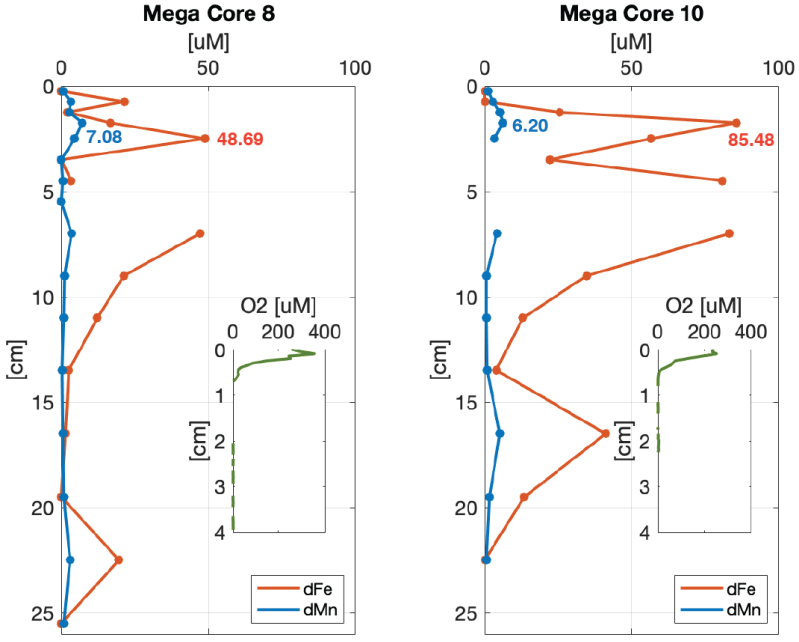

Figure S2. Porewater dissolved metal concentrations for Fe (red), manganese (blue), and oxygen (green) for Mega Core 8 (left) and 10 (right), at the coring station near OB (see Fig. 1).

Date Sampled	Station Name	Latitude [deg N]	Longitude [deg E]	Depth [m]	FIA [nM] dFe	ICPMS [nM] dFe	dMn	TDFe	TDMn
11/27/15	SIII 5	-64.7498	-62.9844	8	2.29				
				35	1.97				
				134	2.93				
11/28/15	MBA	-64.8582	-62.5832	8	2.12				
				25	1.88				
				134	3.77				
				276	8.44				
11/29/15	SIII 3	-64.8407	-62.6176	5	2.08				
				25	1.97				
				109	2.83				
				273	7.06				
11/30/15	IBA	-64.8635	-62.5434	6	2.32				
				15	2.14				
				109	3.26				
				174	4.83				
12/1/15	SIII 4	-64.8149	-62.7378	7	2.01				
				71	2.70				
				191	4.76				
				294	10.09				
12/2/15	IBA	-64.8937	-62.5724	5	1.85			154.91	7.48
				27	1.87	2.52	3.49	170.70	8.33
				174	4.47	5.84	3.56	992.57	22.70
				398	10.87			355.82	12.02
12/3/15	IBB	-64.8783	-62.4146	5	2.51			239.87	9.38
				43	3.48			230.98	6.88
				174	4.69				
12/3/15	SIII 3	-64.8180	-62.6261	11	2.49				
				338	11.86				
12/4/15	SIII 3	-64.8180	-62.6261	11	6.05				
12/4/15	SIII 3	-64.8180	-62.6261	11	3.82				
12/4/15	SIII 3	-64.8180	-62.6261	11	2.25				
				330	15.13				
12/5/15	IBA	-64.8915	-62.6025	5	2.18	2.46	3.50		
				33	2.71	2.81	3.42		
				109	8.60	8.14	4.36		
12/6/15	IBB	-64.8654	-62.4024	6	3.41	3.36	4.40		
				43	3.40	3.29	3.45		
				76	4.88	4.67	3.39		
				218	15.01	9.19	3.49		
12/7/15	MBB	-64.8252	-62.6492	5	2.78				
				56	3.12				
				240	10.22				
12/8/15	SIII 3	-64.8175	-62.6251	4	2.49	2.37	3.25	83.61	5.63
				50	3.72	3.66	3.80	137.58	6.81
				279	17.14	13.55	3.56	211.86	7.51
12/9/15	OBA	-64.7680	-62.7565	5	1.73			104.42	4.62
				37	2.74			90.99	4.42
				109	4.16			102.24	4.16
12/9/15	Gerlache Strait	-64.6607	-62.9274	11	3.44				
				121	1.25				
12/10/15	MBA	-64.8669	-62.5585	4	1.96				
				134	3.92				
12/11/15	IBA	-64.8950	-62.5704	5	2.19				
12/11/15	Gerlache Strait	-64.6613	-62.9283	5	1.31	1.49	2.58	52.27	4.24
				30	1.51	1.61	2.60	35.17	3.53
				110	2.81	3.91	1.85	42.25	2.77
12/12/15	OBB	-64.7738	-62.8663	5	1.95	2.50	2.98		
				30	2.33	2.96	3.06		
				110	3.58	3.87	2.37		
12/12/15	SIII 3	-64.8257	-62.6204	10	3.40				
				100	4.76				
12/13/15	SIII 3	-64.8255	-62.6141	10	3.12				
12/13/15	SIII 3	-64.8248	-62.6155	10	3.29				
12/13/15	SIII 3	-64.8261	-62.6176	10	3.78				
				90	4.53				
12/14/15	Errera Strait	-64.7520	-62.7026	5	1.53				
				35	2.36				
				100	2.98				
12/16/15	IBA	-64.8936	-62.5737	5	2.01				
				50	3.05				
				344	7.28				
12/17/15	SIII 3	-64.8348	-62.6089	4	1.61				
12/18/15	SIII 4	-64.8095	-62.6908	5	5.52				
12/20/15	Station B	-64.7732	-65.3177	5	2.07				
				300	1.57				
4/6/16	SIII 4	-64.8072	-62.7027	25	6.93				
				80	8.35				
				150	13.93				
				300	9.03				
4/7/16	IBA	-64.8812	-62.5598	25	7.80				
				80	8.51				
4/8/16	Andvord Front	-64.7990	-62.7525	15	4.69	4.69	4.46		
				120	5.37	5.10	4.24		
4/9/16	Errera Strait	-64.7525	-62.6993	25	5.49	5.45	4.54	108.95	6.37
				100	-	8.78	5.37	207.99	7.98
4/10/16	MBA	-64.8606	-62.5837	20	6.16				
				60	6.27				
				300	12.35				
4/11/16	IBB	-64.8752	-62.4044	20	8.48	6.89	6.81	383.25	15.34
				75	5.76	5.94	5.87	330.75	13.11
				250	7.68	7.70	6.76	227.84	12.17
4/11/16	SIII 3	-64.8380	-62.6106	15	4.61	5.41	5.17	131.97	8.69
				75	4.53	5.20	4.65	141.41	7.97
				250	5.69	6.22	4.49	89.42	6.09
4/11/16	OBA	-64.7657	-62.7057	15	4.89	5.44	4.80	122.35	6.94
				80	4.51	4.99	4.01	81.36	5.44
				250	6.00	6.82	4.54	138.19	7.14
4/11/16	Gerlache Strait	-64.6590	-62.9255	15	5.14	5.27	3.90	101.84	6.07
				80	4.83	5.12	4.09	96.21	5.21
				250	5.16	5.59	4.07	104.76	6.70
4/12/16	Andvord Front	-64.8224	-62.6941	15	5.29				
				40	5.43				
				250	7.20				
4/13/16	SIII 1.5	-64.8608	-62.5378	15	8.23				
				125	6.92				
4/14/16	MBB	-64.8258	-62.6472	15	7.83				
				80	6.96				
				200	8.12				
4/14/16	MBA	-64.8734	-62.5605	60	12.69				
4/16/16	SIII 3	-64.8323	-62.6004	15	7.78				
				75	6.90				
				250	7.91				
4/16/16	IBA	-64.8925	-62.5825	20	9.15	9.67	5.54	308.83	13.84
				100	10.84	11.64	5.82	419.88	15.73
				280	12.88	14.45	9.43	683.63	23.46
4/17/16	IBA	-64.8922	-62.5738	20	6.08	6.54	5.67	248.94	12.72
				100	9.01	9.40	6.22	538.33	17.28
				280	11.56	10.51	9.18	502.70	18.48
				500	14.25	12.41	15.79	879.48	34.96
4/18/16	IBB	-64.8728	-62.4315	20	8.09				
				75	7.43				
				240	7.97				
4/19/16	OBB	-64.7736	-62.8663	15	6.61				
				100	5.96				
				280	16.34				
4/20/16	SIII 1	-64.8752	-62.4538	15	6.98				
				150	6.07				
				280	11.41				
4/21/16	SIII 5.5	-64.7385	-62.9666	20	6.50				
				67	4.90				
				280	4.51				
4/22/16	IBA	-64.9003	-62.5780	110	7.54	7.26	5.28	277.24	11.63
4/22/16	IBA	-64.8834	-62.5590	110	6.87	6.72	4.79	202.34	10.36
4/26/16	Station B	-64.8167	-65.3537	20	1.97	1.91	2.32	30.51	2.99
4/26/16				150	2.04	1.85	1.27	15.40	1.93
4/26/16				400	1.94	1.79	0.73	28.75	1.82

Table S1. Seawater samples: Fe, Mn determined for the dissolved (dTM, 0.2 µm) and the total dissolvable (TDTM) determined by FIA and ICPMS methods, and collected during LMG1510 and NBP1604. Additional information covers sampling date, location (station), and latitude and longitude.

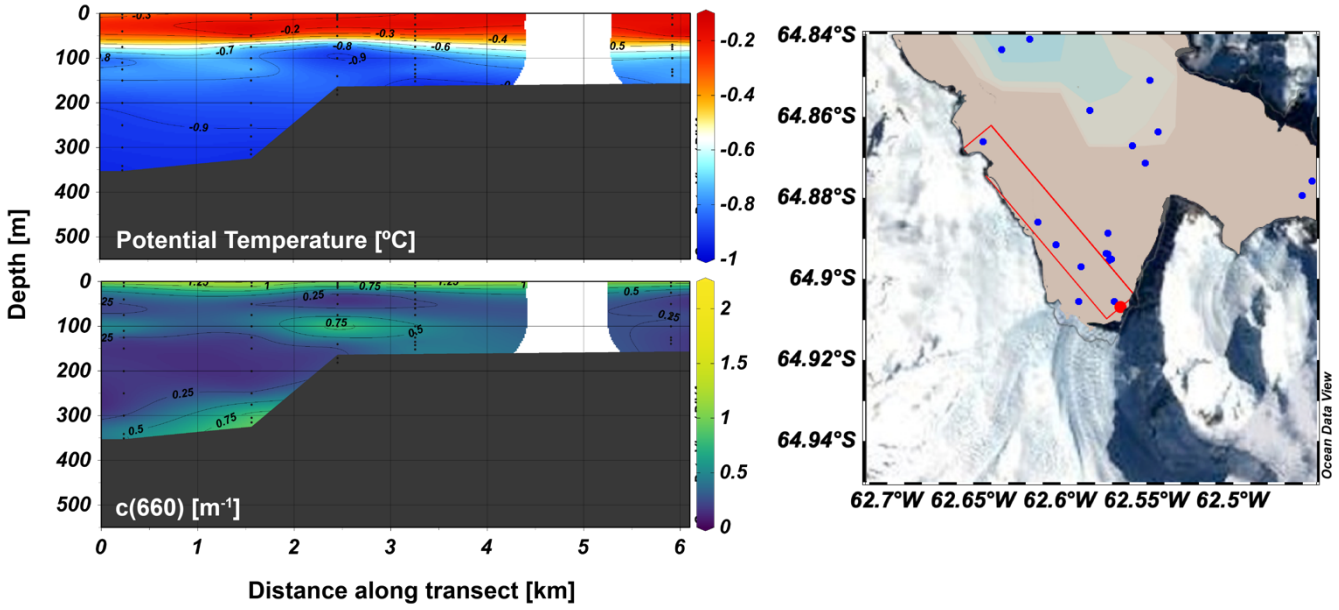

Figure S3. Bagshawe Glacier CTD transect during LMG1510 (late Spring) showing temperature (top panel) and beam attenuation coefficient at 660 nm (bottom panel). Section plots are oriented as if facing the coast. The transect is highlighted by a red box on the map. (Plots were made with Ocean Data View visualization software (Schlitzer, 2002, Ocean Data View, last access: 1 February 2021).

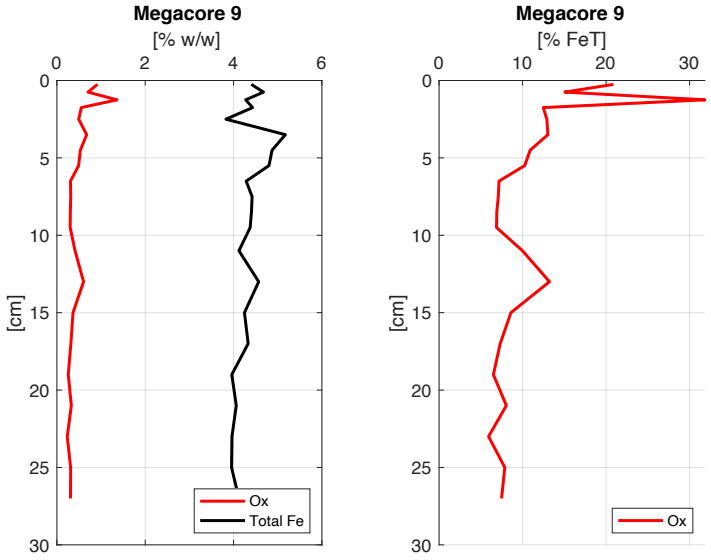

Figure S4. Speciation of Andvord Bay sediments as percent dry sediment weight (left) and percent total Fe (right) for defined fractions based on chemical lability, as in Burdige *et al.* (2020). Ox = oxides.

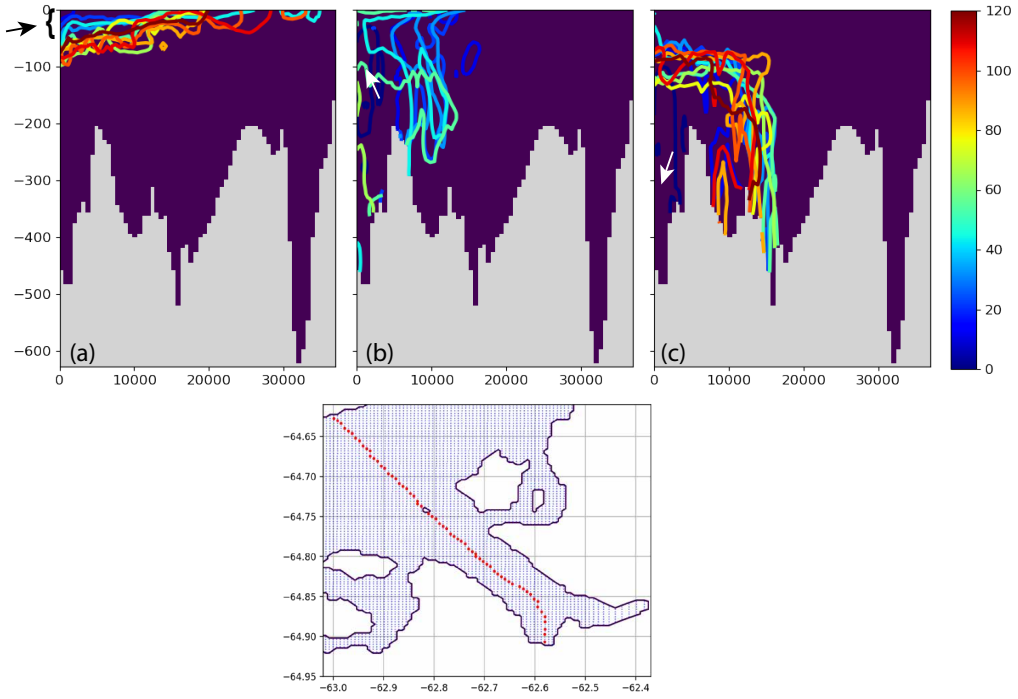

Figure S5. Modeled fate of numerical dyes representing three possible Fe sources. Contours show the 0.1% extent for the (a) meltwater dye and the 0.01% extent of the (b) subsurface, and (c) deep dyes according to the day in the model run (colorbar). Approximate dye release depth and location are highlighted by the arrows. The plots are oriented from the inner basins (0 m) to the Gerlache Strait (~35000 m) as distance from Bagshawe Glacier ([m]).

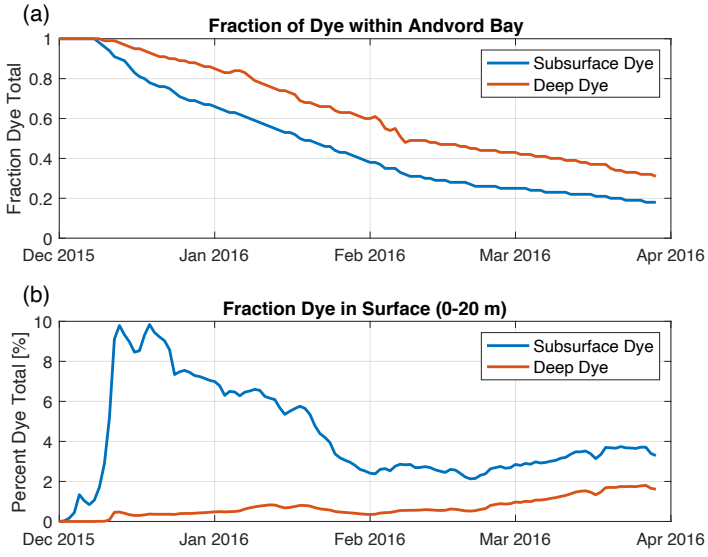

Figure S6. (a) Fraction of initial subsurface (blue) and deep (orange) numerical dye within the fjord domain over the 120-day model run. (b) Percentage of subsurface and deep dye within the surface layer (0-20m) over the 120-day model run.

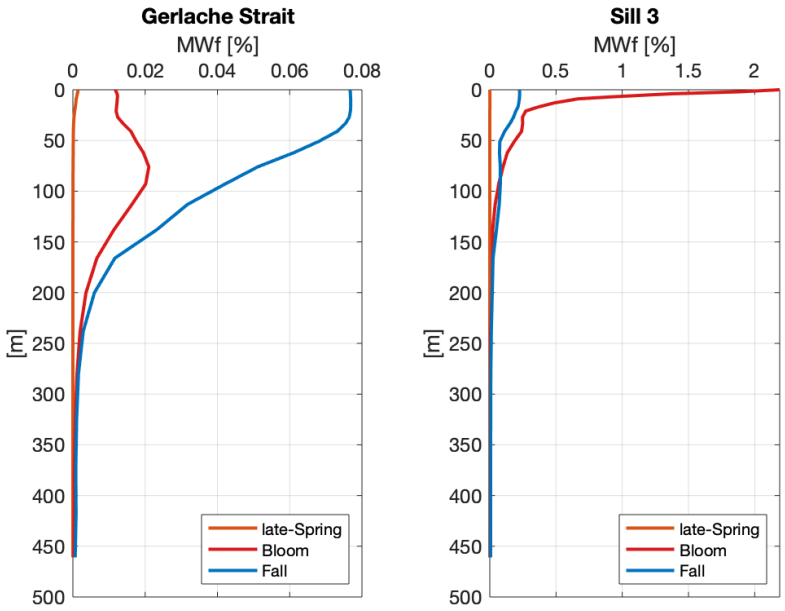

Figure S7. Modeled meltwater dye profiles as a percent of water volume in the (left) Gerlache Strait and (right) Sill 3. Each profile corresponds to a different timepoint: late Spring (December 11, 2015 Gerlache, December 3, 2015 Sill 3), peak bloom period (January 27, 2016), and simulation end (March 29, 2016). Note the different x-scales.

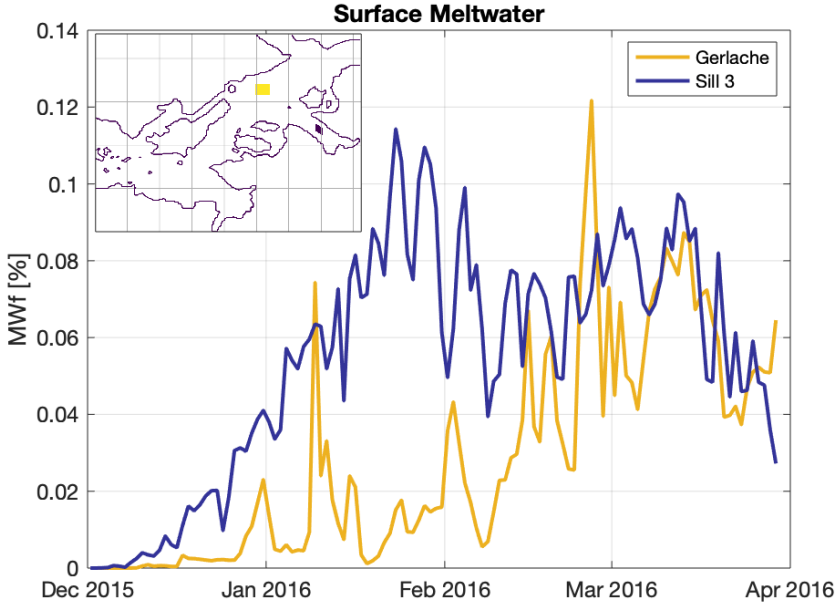

Figure S8. Modeled surface (0-20m) meltwater fraction for Gerlache Strait and Sill 3 (map inset), over the course of the 2015-16 summer season.

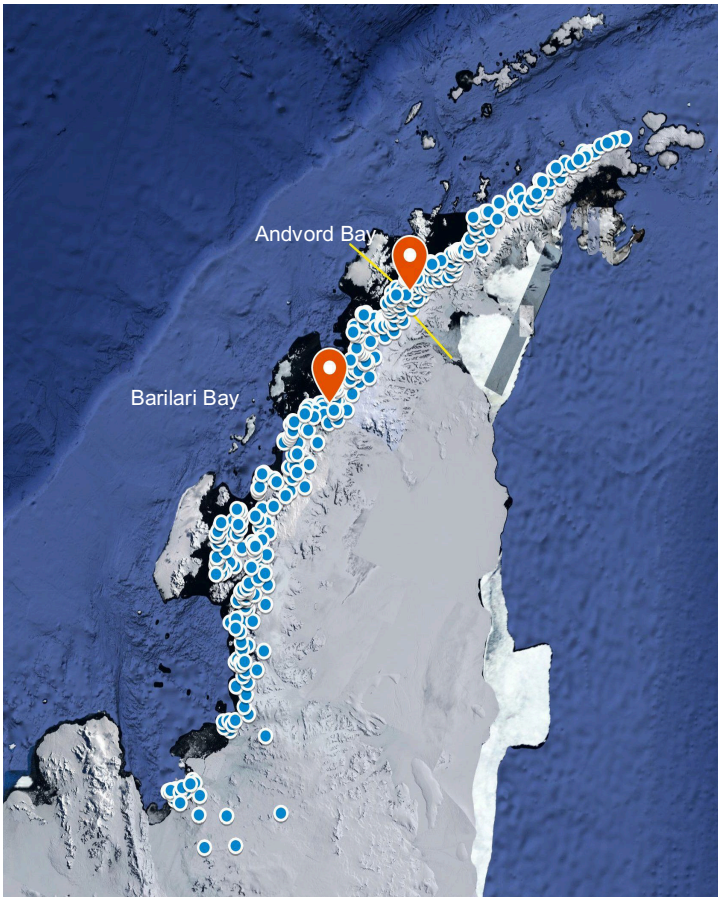

Figure S9. Map showing all 432 glaciers (blue dots) located on the western coast of the WAP (from Cook *et al.,* 2016). The yellow line indicates the region of convergence of two intermediate water masses; cold Weddell Water to the north and warm modified UCDW to the south. Image was produced using *Google Maps*, 10 January 2021.

References

Hahn-Woernle, L. *et al.* (2020) 'Sensitivity of the summer upper ocean heat content in a Western Antarctic Peninsula fjord', *Progress in Oceanography*, 183, p. 102287. doi: https://doi.org/10.1016/j.pocean.2020.102287.

Jordan, T. A., Riley, T. R. and Siddoway, C. S. (2020) 'The geological history and evolution of West Antarctica', *Nature Reviews Earth & Environment*, 1(2), pp. 117–133. doi: 10.1038/s43017-019-0013-6.